GEOLOGY | THE GEOLOGICAL SOCIETY OF AMERICA®

https://doi.org/10.1130/G45924.1

Manuscript received 14 December 2019
Revised manuscript received 23 June 2020
Manuscript accepted 28 June 2020

Published online 31 July 2020

Oxidative conditions can lead to exceptional preservation through phosphatization

Pierre Gueriau[1,2,3]*, Sylvain Bernard[4], François Farges[4], Cristian Mocuta[1], Didier B. Dutheil[5], Thierry Adatte[3], Brahimsamba Bomou[3], Marie Godet[2], Dominique Thiaudière[1], Sylvain Charbonnier[5] and Loïc Bertrand[2,1,6]

[1]Synchrotron SOLEIL, l'Orme des Merisiers, BP 48 Saint-Aubin, 91192 Gif-sur-Yvette, France
[2]Université Paris-Saclay, CNRS, Ministère de la culture, UVSQ, MNHN, Institut photonique d'analyse non-destructive européen des matériaux anciens (IPANEMA), 91192, Saint-Aubin, France
[3]Institute of Earth Sciences, University of Lausanne, Géopolis, CH-1015 Lausanne, Switzerland
[4]Muséum National d'Histoire Naturelle (MNHN), Sorbonne Université, CNRS UMR 7590, Institut de Minéralogie, de Physique des Matériaux et de Cosmochimie (IMPMC), 75005 Paris, France
[5]Muséum National d'Histoire Naturelle (MNHN), Sorbonne Université, CNRS UMR 7207, Centre de Recherche en Paléontologie–Paris (CR2P), 8 rue Buffon, 75005 Paris, France
[6]Université Paris-Saclay, ENS Paris-Saclay, CNRS, PPSM, 91190, Gif-sur-Yvette, France

ABSTRACT

Exceptional preservation through phosphatization is primarily controlled by a reduction in pH, favoring the precipitation of apatite over that of calcite. Laboratory experiments have suggested that phosphatization results from anoxic decay. Here we report results of the fine-scale mineralogical characterization of Cretaceous phosphatized fossils of teleost fishes and crustaceans from the Jebel oum Tkout Lagerstätte (Morocco). Data collected using complementary laboratory and synchrotron-based X-ray techniques reveal that oxidative conditions were established at a certain step of decay. Supporting these conclusions are the presence, covering and embedded in the phosphatized tissues, of Fe(III)-rich mineral phases, the precipitation of which was likely biologically induced during decay. The present study highlights that the establishment of oxidative conditions during decay can be compatible with exceptional preservation of fossils through phosphatization.

INTRODUCTION

Soft-tissue phosphatization, i.e., calcium phosphate mineralization occurring prior to the degradational collapse of cellular tissues, provides the most spectacular fossils of animals, still exhibiting subcellular details (Martill, 1990; Briggs, 2003). Most of the time, soft tissues are pseudomorphically replaced by francolite (a carbonate-rich fluorapatite), as is the case of the iconic ca. 110 Ma fossil fishes from the Santana Formation (Brazil) (Martill, 1988). Laboratory experiments have suggested that phosphatization results from a decay-induced fall in pH under anaerobic conditions, the decrease of pH being responsible for a switch from carbonate to phosphate precipitation (Allison, 1988; Briggs and Kear, 1993; Briggs and Wilby, 1996; Sagemann et al., 1999). However, authigenic phosphates such as francolite may precipitate under a range of redox conditions, including oxic to suboxic conditions (Föllmi, 1996, and references therein). Phosphatization also requires a sufficient concentration of phosphorus (Martill, 1988; Briggs and Kear, 1993; Briggs, 2003). Closed systems, such as those built by biofilms growing around carcasses, promote apatite precipitation by trapping phosphorus (Williams and Reimers, 1983; Martill, 1988; Briggs and Kear, 1993; Wilby et al., 1996), which is released by organic-matter degradation under oxic conditions (e.g., Meunier-Christmann et al., 1989; Mort et al., 2007). Here, we investigate phosphatization from a fossil perspective. We report an in-depth and in situ assessment of the redox conditions having prevailed during the phosphatization of "exceptionally preserved" Cretaceous fossils of fishes and crustaceans from the Jebel oum Tkout (OT1) Lagerstätte of Morocco.

METHODS

A combination of advanced characterization tools, associating mass spectrometry, X-ray diffraction (XRD), scanning electron microscopy, and infrared (IR) spectroscopy with synchrotron-based methods, was used to achieve a micro-geochemical characterization of a series of fossils from the OT1 Lagerstätte. Major-to-trace elemental composition was determined using synchrotron-based micro–X-ray fluorescence (μXRF) mapping at a spatial resolution of 60–100 μm and at detection limits of a few tens of parts per million (Gueriau et al., 2014, 2018). Samples were scanned in air using a 17.2 keV beam. Under these conditions, the μXRF signal originates from the first hundreds of microns, and absorption by the air of low-energy photons from light elements such as phosphorus narrows the detection to elements from chlorine to uranium (see Gueriau et al., 2018). The spectral decomposition of μXRF data allowed estimating the concentrations of all detected elements, including of rare earth elements (REEs) that were then normalized to the post-Archean Australian shale (PAAS) reference (McLennan, 1989) to reconstruct REE patterns, ratios, and anomalies in the fossils at "local", submillimeter scales (Gueriau et al., 2015). Finally, the redox states of Fe and Ce were determined using synchrotron-based micro–X-ray absorption spectroscopy (μXAS) at a 3–10 μm spatial resolution. For Fe, continuous Cauchy wavelet transformation of the spectra was performed to establish a more robust determination of

*E-mail: pierre.gueriau@unil.ch

CITATION: Gueriau, P., et al., 2020, Oxidative conditions can lead to exceptional preservation through phosphatization: Geology, v. 48, p. 1164–1168, https://doi.org/10.1130/G45924.1

the speciation (Muñoz et al., 2003). Additional information on methods is provided in the Supplemental Material[1].

GEOLOGICAL AND PALEOENVIRONMENTAL CONTEXT

The Upper Cretaceous (Cenomanian, ca. 95 Ma) OT1 Lagerstätte from southeastern Morocco (Fig. 1A) yielded a rich and well-preserved soft-bodied fauna including mollusks, insects, crustaceans, elasmobranchs, and actinopterygian fishes embedded in a pale beige laminated mudstone carved by mudcracks (Fig. 1B). Absence of marine organisms and the presence of mudcracks, unionids, and larvae of insects restricted to freshwater environments strongly suggest a low-energy seasonally dried freshwater deposition environment (Dutheil, 1999; Garassino et al., 2006). A paleoenvironmental model of the whole Kem Kem area is available in Ibrahim et al. (2020).

MINERALOGY

Remarkably, many fossils exhibit soft tissues (muscles, cuticles, and gills; Figs. 1C–1E; Dutheil, 1999; Garassino et al., 2006; Gueriau et al., 2015) pseudomorphically replaced by nanometric apatite crystallites (<30 nm), identified as francolite by infrared spectroscopy (Fig. 1F). XRD analyses on oriented preparations show that the mineralogy of the sedimentary matrix is dominated by illite and quartz, with some illite-smectite mixed layers and kaolinite. These minerals are mainly detrital, except for the accordion-like automorphic crystals of kaolinite. Low trace-metal concentrations (Fig. S1C in the Supplemental Material) with very low degrees of enrichment (PAAS-normalized enrichment factors for V, Ni, Cu, Zn ≤ 1.1, Cr ~1.9) and chemical index of alteration of ~78 (Nesbitt and Young, 1982; low range for illite) indicate very moderate weathering. Gypsum filling mudcracks (Fig. 1B), halite crystals locally found on the sample surface (Figs. S2L, S2 M, and S2P), and Fe-rich clay minerals displaying plate-like or sheet-like habits forming roses on the sample surface (Figs. S2G–S2J, S2N, and S2O) are clearly secondary (and rather recent), indicating that sampling and storage conditions may have slightly altered the samples.

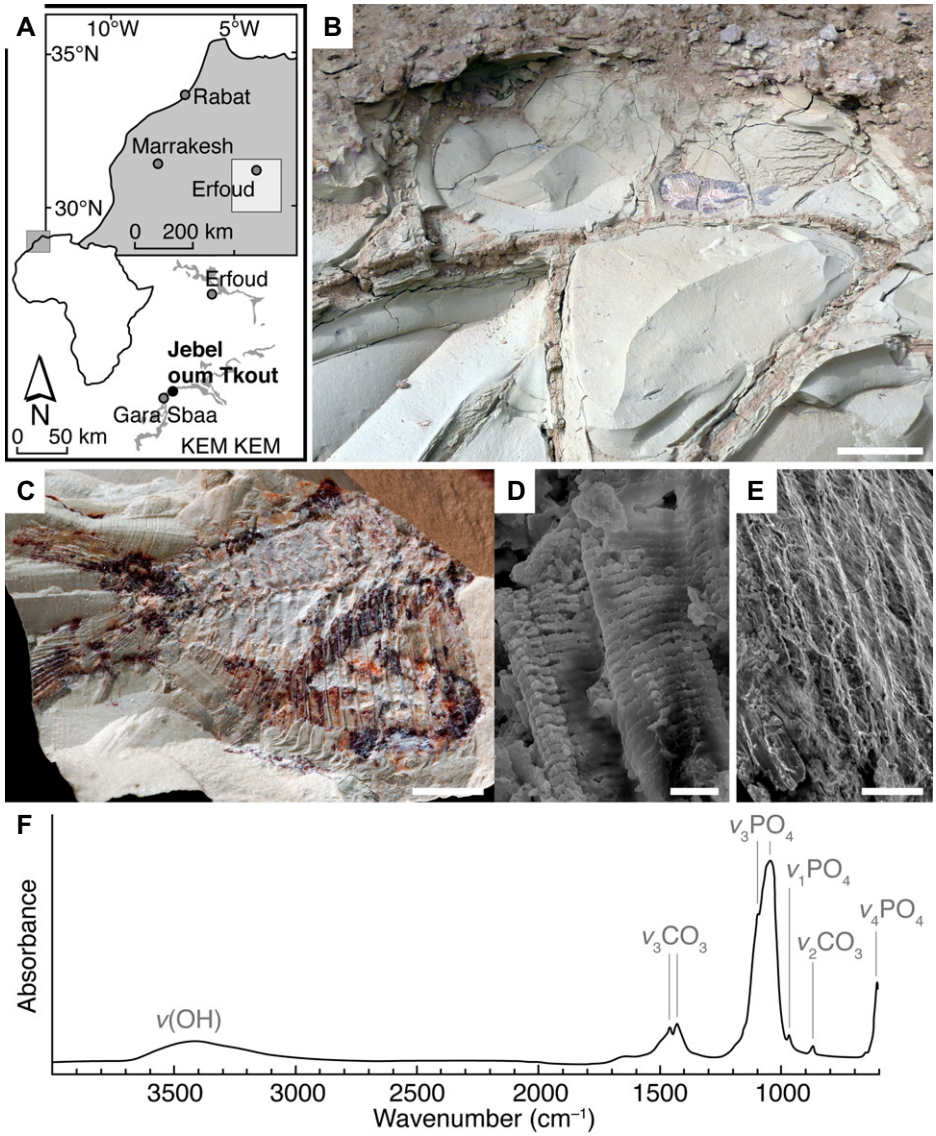

Figure 1. Jebel oum Tkout (OT1) Lagerstätte (Cenomanian, Morocco). (A) Location and map of the Kem Kem area, southeastern Morocco; gray areas denote outcrops of Kem Kem beds. Note the presence of another, slightly younger and marine Lagerstätte at Gara Sbaa (Martill et al., 2011), ~15 km southwest of the OT1 Lagerstätte. (B) Optical photograph of gray clay layer exhibiting mudcracks and topped by reddish microbial mat. In the center, a paraclupeid fish is visible. (C,D) Optical photograph of another paraclupeid (sample Poi-SGM 10) and scanning electron microscopy (SEM) image (secondary electron mode) of its finely phosphatized muscles (after Dutheil, 1999, his figures 5 and 6). (E) SEM image (secondary electron mode) of mineralized muscles from penaeid shrimp *Cretapenaeus berberus* (sample MNHN.F.A24633) (after Garassino et al., 2006, their figure 5). (F) Infrared spectrum of mineralized muscles from *C. berberus*. *v*—vibrational mode number. Scale bars: B, 5 cm; C, 5 mm; D, 10 μm; E, 50 μm.

REMAINS OF BIOFILMS

Long known for promoting apatite precipitation by trapping phosphorus (Williams and Reimers, 1983; Martill, 1988; Briggs and Kear, 1993; Wilby et al., 1996), fossil biofilms can be observed at the OT1 Lagerstätte. They consist of large (tens of square centimeters) reddish cracked films lying a few millimeters above each of the fossiliferous layers (Fig. 2A). The morphological similarities between these films (Figs. 2B–2D) and modern microbial mats (Fig. 2E) strengthen their identification as well-preserved fossil colonies of microorganisms. A few hundred milligrams of fossil biofilm materials were extracted and milled into powder for XRD analyses, revealing that these large biofilms are composed of Fe_2O_3 [Fe(III) oxide] minerals (Fig. 2F).

Moreover, the fossil skeletons, cuticles, and soft tissues (white to yellowish in color) are largely covered by similar reddish (to sometimes bluish) thin (a few tens of micrometers) patches (Figs. 1B, 1C, and 3A; Fig. S2A) that are interpreted as remains of biofilms. Reddish patches are also found embedded within the phosphatized soft tissues (Figs. 3C–3F; Fig. S3C), suggesting that their precipitation was concomitant with phosphatization. μXRF mapping reveals that these thin biofilm patches

[1]Supplemental Material. Methods; additional synchrotron X-ray fluorescence maps, spectra, and main elemental contributions; REE patterns; Ce L3-edge spectra; Fe K-edge continuous Cauchy wavelet transforms modulus; SEM images; and precise locations of the point analyses. Please visit https://doi.org/10.1130/GEOL.S.12659936 to access the supplemental material, and contact editing@geosociety.org with any questions.

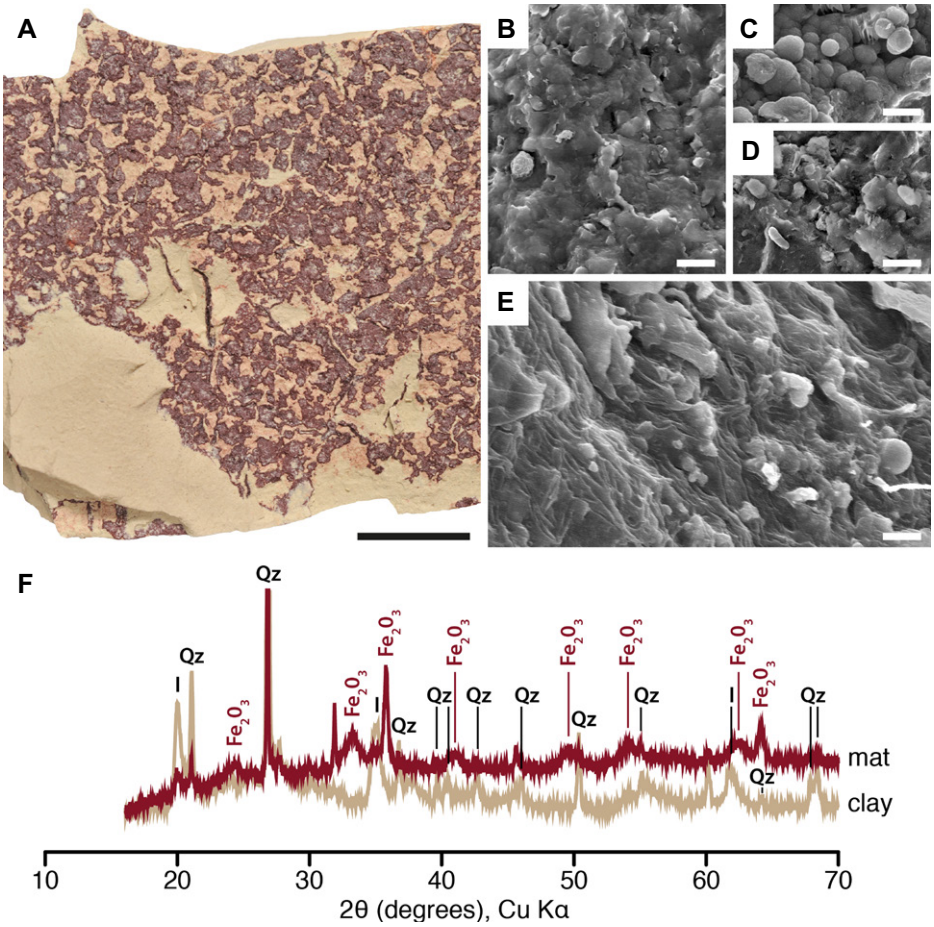

Figure 2. Fossil microbial mats from the Jebel oum Tkout (OT1) Lagerstätte (Cenomanian, Morocco). (A) Optical photograph of OT1 microbial mat. (B–D) Scanning electron microscopy (SEM) images (secondary electron mode) of OT1 microbial mats. (E) SEM image (secondary electron mode) of a modern microbial mat for comparison. (F) X-ray powder diffraction diagrams of fossil mat (mat) and of clayey sedimentary matrix (clay). Qz—quartz; I—illite. Scale bars: A, 1 cm; B–E, 10 µm.

are iron rich and contain trace metals (Figs. 3A, 3B, and 3G; Figs. S1 and S3). µXAS investigations at the Fe K-edge reveal that the chemical speciation of iron in these patches is identical to that of iron in the large biofilms and confirms the presence of Fe(III) (Fig. 3H). The spectrum of this Fe-rich mineral is rather inconsistent with hematite (α-Fe_2O_3) or illite {$(K,H_3O)(Al,Mg,Fe)_2(Si,Al)_4O_{10}[(OH)_2,(H_2O)]$} and less consistent with goethite [α-FeO(OH)] or lepidocrocite [γ-FeO(OH)], while it is consistent with ferrihydrite ($Fe_2O_3 \cdot 0.5H_2O$) (Figs. 3H and 3I; Fig. S4).

AGE AND FORMATION OF THE IRON OXIDES

The observed Fe(III) hydroxides surround skeleton tissues and are found around and within the phosphatized soft tissues (Figs. 3C–3F; Fig. S3C), suggesting that they precipitated concomitantly with phosphatization. Although Fe-rich phases found in association with fossils elsewhere have been interpreted as resulting from the oxidation of pyrite, as attested by pseudomorph minerals or molds left in the surrounding matrix (e.g., Gabbott et al., 2004; Osés et al., 2016), this is not the case for the Fe(III) hydroxides observed in our samples. Instead of a cubic or framboidal habit, typical of pyrite weathering products, the observed Fe(III) hydroxides show a honeycomb-like morphology (Figs. 3E and 3F; Fig. S2), rather typical of microbial mats (e.g., Frankel and Bazylinski, 2003; Davies et al., 2016). In particular, one can observe spherical imprints, possibly created by coccoid-shaped bacteria (e.g., Iniesto et al., 2016) or gas bubbles having been produced within the microbial mats (e.g., Davies et al., 2016). The fossil biofilms discussed here have thus not been exposed to significant weathering or recrystallization. In other words, the observed Fe(III) hydroxides are likely primary, i.e., they precipitated during the life of the microbial mats, thereby indicating slightly oxic conditions during phosphatization.

SUBSEQUENT REDOX CONDITIONS

Synchrotron-based µXRF analyses of the phosphatic fossil tissues reveal that they incorporated REEs, strontium, and thorium, which substitute for calcium in apatite minerals (Fig. 3G). The notable incorporation of REEs occurs after decay, with concentrations increasing by three to four orders of magnitude in 10^3–10^4 yr depending on diagenetic conditions (Herwartz et al., 2013). The obtained REE patterns display a very limited enrichment in intermediate REEs ("bell-shaped" patterns) and a slightly negative Ce anomaly (Fig. S5A; Gueriau et al., 2015). The PAAS-normalized La/Yb versus La/Sm values confirm that the fossils investigated underwent very limited weathering and recrystallization (Fig. 3J; Reynard et al., 1999; Lécuyer et al., 2003). The observed negative Ce anomaly thus reflects early diagenetic redox conditions (German and Elderfield, 1990) and indicates that slightly oxic conditions persisted after decay. Ce L_3-edge spectroscopy confirms that Ce has a mixed valence (Gueriau et al., 2015), with oxidized Ce [i.e., Ce(IV)] contributing to 20 at% of the total Ce (Fig. S5B).

CONCLUSION

Instead of a fall in pH under anoxic conditions, the fine-scale micro-geochemical characterization conducted here strongly suggests that (slightly) oxic conditions prevailed during phosphatization in the OT1 Lagerstätte. This conclusion is consistent with some of the latest experiment results evidencing that chemical microenvironments generated by microbial mats may turn oxic after several weeks despite initially anoxic conditions (Iniesto et al., 2015). One could argue that the observed Fe(III) hydroxides may have been produced by anaerobic neutrophilic iron oxidizers (e.g., Miot et al., 2009; Hedrich et al., 2011). This would not be inconsistent with the present interpretation, i.e., the establishment of slightly oxic conditions during phosphatization, because neutrophilic iron oxidizers require the presence of nitrates to survive, i.e., slightly oxic conditions (anaerobic and anoxic are not strict synonyms). Altogether, the present results establish that exceptional preservation through phosphatization and oxidative conditions are not antithetic.

ACKNOWLEDGMENTS

We acknowledge SOLEIL synchrotron (Saint-Aubin, France) for provision of beamtime under project 20131308. J.-G. Bréhéret (Université de Tours, Tours, France) performed and interpreted the XRD analyses on the bulk sediment. V. Beltran and J. Kaddissy (IPANEMA, France) performed infrared spectroscopy. We thank S. Blanchandin (SOLEIL) for assistance with X-ray powder diffraction of the fossils; D. Vantelon and N. Trcera at the LUCIA beamline (SOLEIL Synchrotron); and teams at the Institut des Sciences Analytiques (UMR 5280 CNRS, Lyon, France) and Service d'Analyze des Roches et des Minéraux (CRPG, UMR 7358 CNRS-INSU, Vandœuvre-lès-Nancy, France) for carrying out the mass-spectrometry measurements. The 2012 field expedition and measurements were supported by the Muséum national d'Histoire naturelle, France (MNHN) through the "ATM Biodiversité actuelle et fossile" and by the UMR 7207 CR2P. We thank the organizers and field workers of the expedition. This work was developed as part of the IPANEMA-MNHN

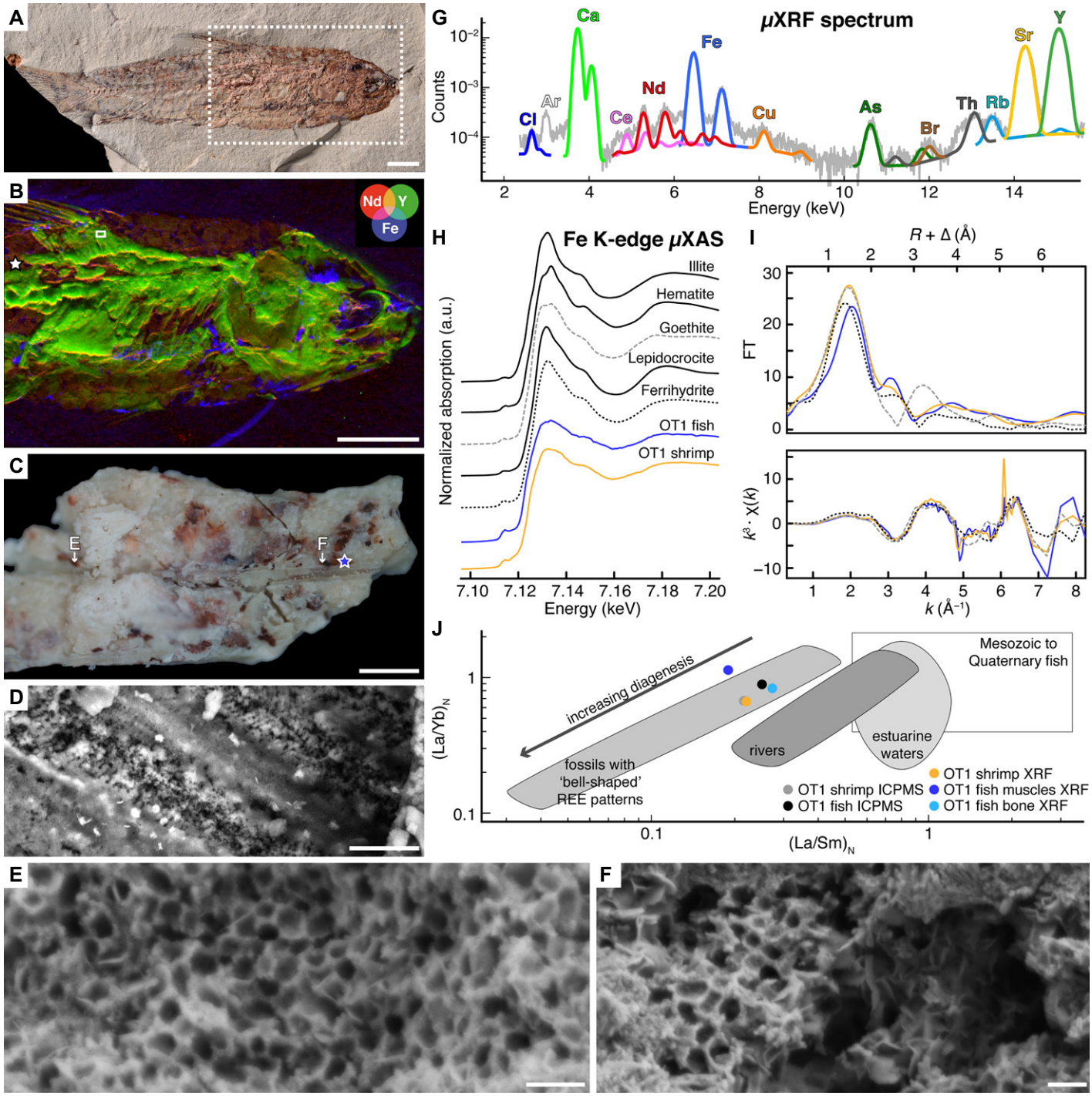

Figure 3. Synchrotron-based micro–X-ray fluorescence (μXRF) mapping and Fe K-edge micro–X-ray absorption spectroscopy (μXAS) from fossils of the Jebel oum Tkout (OT1) Lagerstätte (Cenomanian, Morocco). (A) Optical photographs of teleost fish sample MHNM-KK-OT 10. (B) False-color overlays of neodymium (red), yttrium (green), and iron (blue) distributions from area of dotted white box in A. (C) Optical photograph of loose sample containing soft tissues and bone from sample MHNM-KK-OT 10 (origin: white star in B). (D) Scanning electron microscopy (SEM) image (backscattered electrons mode) of muscle fibers preserved on sample in C. (E–F) SEM images (secondary electron mode) of honeycomb-like iron oxides (origin: arrows in C). (G) Average μXRF spectrum and main elemental contributions from fish dorsal fin muscles (white box in B). (H) Normalized μXAS spectra at Fe K-edge of reference materials (illite, hematite, goethite, lepidocrocite, and ferrihydrite) and of iron-rich grains covering teleost fish (origin: blue star in C) and penaeid shrimp *Cretapenaeus berberus* (sample MHNM-KK-OT 01; see Fig. S3 [see footnote 1]). Spectra were vertically shifted for increased readability. (I) Fourier transform (FT) magnitude and k^3-weighted μXAS spectra from iron-rich grains covering teleost fish (blue) and shrimp (orange), as well as ferrihydrite (dotted black) and goethite (dotted gray) reference materials. (J) Post-Archean Australian shale (PAAS)–normalized La/Yb ratios versus La/Sm ratios in OT1 fossils from μXRF and inductively coupled plasma–mass spectrometry (ICPMS) quantifications reported in diagrams proposed by Reynard et al. (1999); gray areas from Lécuyer et al. (2003). REE—rare earth element. Scale bars: A–B, 5 mm; C, 500 μm; D, 10 μm; E–F, 1 μm.

agreement on collaborative research. We thank Paul Wilson and the anonymous reviewers for constructive suggestions to improve the quality of this manuscript.

REFERENCES CITED

Allison, P.A., 1988, The role of anoxia in the decay and mineralization of proteinaceous macro-fossils: Paleobiology, v. 14, p. 139–154, https://doi.org/10.1017/S009483730001188X.

Briggs, D.E.G., 2003, The role of decay and mineralization in the preservation of soft-bodied fossils: Annual Review of Earth and Planetary Sciences, v. 31, p. 275–301, https://doi.org/10.1146/annurev.earth.31.100901.144746.

Briggs, D.E.G., and Kear, A.J., 1993, Fossilization of soft tissue in the laboratory: Science, v. 259, p. 1439–1442, https://doi.org/10.1126/science.259.5100.1439.

Briggs, D.E.G., and Wilby, P.R., 1996, The role of the calcium carbonate–calcium phosphate switch in the mineralization of soft-bodied fossils: Journal of the Geological Society, v. 153, p. 665–668, https://doi.org/10.1144/gsjgs.153.5.0665.

Davies, N.S., Liu, A.G., Gibling, M.R., and Miller, R.F., 2016, Resolving MISS conceptions and misconceptions: A geological approach to sedimentary surface textures generated by microbial and abiotic processes: Earth-Science Reviews, v. 154, p. 210–246, https://doi.org/10.1016/j.earscirev.2016.01.005.

Dutheil, D.B., 1999, An overview of the freshwater fish fauna from the Kem Kem beds (Late Cretaceous: Cenomanian) of southeastern Morocco, *in* Arratia, G., and Schultze, H.-P., eds., Mesozoic Fishes 2—Systematics and Fossil Record: Munich, Germany, Verlag Dr. Friedrich Pfeil, p. 553–563.

Föllmi, K.B., 1996, The phosphorus cycle, phosphogenesis and marine phosphate-rich deposits: Earth-Science Reviews, v. 40, p. 55–124, https://doi.org/10.1016/0012-8252(95)00049-6.

Frankel, R.B., and Bazylinski, D.A., 2003, Biologically induced mineralization by bacteria: Reviews in Mineralogy and Geochemistry, v. 54, p. 95–114, https://doi.org/10.2113/0540095.

Gabbott, S.E., Hou, X.-g., Norry, M.J., and Siveter, D.J., 2004, Preservation of Early Cambrian animals of the Chengjiang biota: Geology, v. 32, p. 901–904, https://doi.org/10.1130/G20640.1.

Garassino, A., Pasini, G., and Dutheil, D.B., 2006, *Cretapenaeus berberus* n. gen., n. sp. (Crustacea, Decapoda, Penaeida) from the Late Cretaceous (Cenomanian) of southeastern Morocco: Atti della Società Italiana di Scienze Naturali e del Museo Civico Naturale di Milano, v. 147, p. 3–17.

German, C.R., and Elderfield, H., 1990, Application of the Ce anomaly as a paleoredox indicator: The ground rules: Paleoceanography, v. 5, p. 823–833, https://doi.org/10.1029/PA005i005p00823.

Gueriau, P., Mocuta, C., Dutheil, D.B., Cohen, S.X., Thiaudière, D., the OT1 consortium, Charbonnier, S., Clément, G., and Bertrand, L., 2014, Trace elemental imaging of rare earth elements discriminates tissues at microscale in flat fossils: PLoS One, v. 9, e86946, https://doi.org/10.1371/journal.pone.0086946.

Gueriau, P., Mocuta, C., and Bertrand, L., 2015, Cerium anomaly at microscale in fossils: Analytical Chemistry, v. 87, p. 8827–8836, https://doi.org/10.1021/acs.analchem.5b01820.

Gueriau, P., Jauvion, C., and Mocuta, M., 2018, Show me your yttrium, and I will tell you who you are: Implications for fossil imaging: Palaeontology, v. 61, p. 981–990, https://doi.org/10.1111/pala.12377.

Hedrich, S., Schlömann, M., and Johnson, D.B., 2011, The iron-oxidizing proteobacteria: Microbiology, v. 157, p. 1551–1564, https://doi.org/10.1099/mic.0.045344-0.

Herwartz, D., Tütken, T., Jochum, K.P., and Sander, P.M., 2013, Rare earth element systematics of fossil bone revealed by LA-ICPMS analysis: Geochimica et Cosmochimica Acta, v. 103, p. 161–183, https://doi.org/10.1016/j.gca.2012.10.038.

Ibrahim, N., Sereno, P.C., Varrichio, D.J., Martill, D.M., Dutheil, D.B., Unwin, D.M., Baidder, L., Larsson, H.C.E., Zouhri, S., and Kaoukaya, A., 2020, Geology and paleontology of the Upper Cretaceous Kem Kem Group of eastern Morocco: ZooKeys, v. 928, p. 1–216, https://doi.org/10.3897/zookeys.928.47517.

Iniesto, M., Laguna, C., Florín, M., Guerrero, M.C., Chicote, A., Buscalioni, A.D., and López-Archilla, A.I., 2015, The impact of microbial mats and their microenvironmental conditions in early decay of fish: Palaios, v. 30, p. 792–801, https://doi.org/10.2110/palo.2014.086.

Iniesto, M., Buscalioni, Á.D., Guerrero, M.C., Benzerara, K., Moreira, D., and López-Archilla, A.I., 2016, Involvement of microbial mats in early fossilization by decay delay and formation of impressions and replicas of vertebrates and invertebrates: Scientific Reports, v. 6, 25716, https://doi.org/10.1038/srep25716.

Lécuyer, C., Bogey, C., Garcia, J.-P., Grandjean, P., Barrat, J.-A., Floquet, M., Bardet, N., and Pereda-Superbiola, X., 2003, Stable isotope composition and rare earth element content of vertebrate remains from the Late Cretaceous of northern Spain (Laño): Did the environmental record survive?: Palaeogeography, Palaeoclimatology, Palaeoecology, v. 193, p. 457–471, https://doi.org/10.1016/S0031-0182(03)00261-X.

Martill, D.M., 1988, Preservation of fish in the Cretaceous Santana Formation of Brazil: Palaeontology, v. 31, p. 1–18.

Martill, D.M., 1990, Macromolecular resolution of fossilized muscle tissue from an elopomorph fish: Nature, v. 346, p. 171–172, https://doi.org/10.1038/346171a0.

Martill, D.M., Ibrahim, N., Brito, P.M., Baider, L., Zhouri, S., Loveridge, R., Naish, D., and Hing, R., 2011, A new Plattenkalk Konservat Lagerstätte in the Upper Cretaceous of Gara Sbaa, south-eastern Morocco: Cretaceous Research, v. 32, p. 433–446, https://doi.org/10.1016/j.cretres.2011.01.005.

McLennan, S.M., 1989, Rare earth elements in sedimentary rocks: Influence of provenance and sedimentary processes: Reviews in Mineralogy and Geochemistry, v. 21, p. 169–200, https://doi.org/10.1515/9781501509032-010.

Meunier-Christmann, C., Lucas, J., and Albrecht, P., 1989, Organic geochemistry of Moroccan phosphorites and bituminous shales: A contribution to the problem of phosphogenesis: Sciences Géologiques Bulletin, v. 42, p. 205–222, https://doi.org/10.3406/sgeol.1989.1823.

Miot, J., et al., 2009, Iron biomineralization by anaerobic neutrophilic iron-oxidizing bacteria: Geochimica et Cosmochimica Acta, v. 73, p. 696–711, https://doi.org/10.1016/j.gca.2008.10.033.

Mort, H.P., Adatte, T., Föllmi, K.B., Keller, G., Steinmann, P., Matera, V., Berner, Z., and Stüben, D., 2007, Phosphorus and the roles of productivity and nutrient recycling during Oceanic Anoxic Event 2: Geology, v. 35, p. 483–486, https://doi.org/10.1130/G23475A.1.

Muñoz, M., Argoul, P., and Farges, F., 2003, Continuous Cauchy wavelet transform analyses of EXAFS spectra: A qualitative approach: American Mineralogist, v. 88, p. 694–700, https://doi.org/10.2138/am-2003-0423.

Nesbitt, H.W., and Young, G.M., 1982, Early Proterozoic climates and plate motions inferred from major element chemistry of lutites: Nature, v. 299, p. 715–717, https://doi.org/10.1038/299715a0.

Osés, G.L., et al., 2016, Deciphering the preservation of fossil insects: A case study from the Crato Member, Early Cretaceous of Brazil: PeerJ, v. 4, e2756, https://doi.org/10.7717/peerj.2756.

Reynard, B., Lécuyer, C., and Grandjean, P., 1999, Crystal-chemical controls on rare-earth element concentrations in fossil biogenic apatites and implications for paleoenvironmental reconstructions: Chemical Geology, v. 155, p. 233–241, https://doi.org/10.1016/S0009-2541(98)00169-7.

Sagemann, J., Bale, S.J., Briggs, D.E.G., and Parkes, R.J., 1999, Controls on the formation of authigenic minerals in association with decaying organic matter: An experimental approach: Geochimica et Cosmochimica Acta, v. 63, p. 1083–1095, https://doi.org/10.1016/S0016-7037(99)00087-3.

Wilby, P.R., Briggs, D.E.G., Bernier, P., and Gaillard, C., 1996, Role of microbial mats in the fossilization of soft tissues: Geology, v. 24, p. 787–790, https://doi.org/10.1130/0091-7613(1996)024<0787:ROMMIT>2.3.CO;2.

Williams, L.A., and Reimers, C., 1983, Role of bacterial mats in oxygen-deficient marine basins and coastal upwelling regimes: Preliminary report: Geology, v. 11, p. 267–269, https://doi.org/10.1130/0091-7613(1983)11<267:ROBMIO>2.0.CO;2.

Printed in USA